Geophysical Research Letters

RESEARCH LETTER
10.1029/2022GL101921

On the Energy-Dependent Deep ($L < 3.5$) Penetration of Radiation Belt Electrons

Yang Mei[1,2], Xinlin Li[1,2], Hong Zhao[3], Theodore Sarris[4], Lengying Khoo[5], Benjamin Hogan[1,2], Declan O'Brien[1,2], and Sam Califf[6,7]

[1]Laboratory for Atmospheric and Space Physics, University of Colorado, Boulder, CO, USA, [2]Department of Aerospace Engineering Sciences, University of Colorado Boulder, Boulder, CO, USA, [3]Department of Physics, Auburn University, Auburn, AL, USA, [4]Department of Electrical and Computer Engineering, Democritus University of Thrace, Xanthi, Greece, [5]Department of Astrophysical Sciences, Princeton University, Princeton, NJ, USA, [6]CIRES, University of Colorado, Boulder, CO, USA, [7]National Centers for Environmental Information, Boulder, CO, USA

Key Points:

- Convective radial transport of storm-time enhanced large-scale *E*-fields is an efficient inward transport mechanism of 10–100 s keV electrons
- The energy-dependent electron penetration can be explained by the relation between the timescales of electron drift and large-scale *E*-fields
- A radial diffusion-convection model is developed to reproduce the storm-time penetration of lower energy electrons to lower *L*

Supporting Information:

Supporting Information may be found in the online version of this article.

Correspondence to:

Y. Mei,
yang.mei@colorado.edu

Citation:

Mei, Y., Li, X., Zhao, H., Sarris, T., Khoo, L., Hogan, B., et al. (2023). On the energy-dependent deep ($L < 3.5$) penetration of radiation belt electrons. *Geophysical Research Letters*, *50*, e2022GL101921. https://doi.org/10.1029/2022GL101921

Received 31 OCT 2022
Accepted 15 MAR 2023

Author Contributions:

Conceptualization: Xinlin Li, Hong Zhao
Formal analysis: Yang Mei, Xinlin Li, Hong Zhao
Investigation: Yang Mei
Methodology: Yang Mei, Xinlin Li, Hong Zhao, Theodore Sarris, Lengying Khoo
Project Administration: Xinlin Li
Resources: Yang Mei
Software: Yang Mei
Supervision: Xinlin Li
Visualization: Theodore Sarris
Writing – original draft: Yang Mei

Abstract Deep penetration of outer radiation belt electrons to low *L* (<3.5) has long been recognized as an energy-dependent phenomenon but with limited understanding. The Van Allen Probes measurements have clearly shown energy-dependent electron penetration during geomagnetically active times, with lower energy electrons penetrating to lower *L*. This study aims to improve our ability to model this phenomenon by quantitatively considering radial transport due to large-scale azimuthal electric fields (*E*-fields) as an energy-dependent convection term added to a radial diffusion Fokker-Planck equation. We use a modified Volland-Stern model to represent the enhanced convection field at lower *L* to match the observations of storm time values of *E*-field. We model 10–400 MeV/G electron phase space density with an energy-dependent radial diffusion coefficient and this convection term and show that the model reproduces the observed deep penetrations well, suggesting that time-variant azimuthal *E*-fields contribute preferentially to the deep penetration of lower-energy electrons.

Plain Language Summary Electrons trapped by the Earth's magnetic field gather in two regions known as the Van Allen radiation belts. It is well reported that electrons can be transported radially inward from the outer radiation belt during geomagnetically active times. More specifically, low energy (100 s of keV) electrons can be moved radially deeper than higher energy (~1 MeV) electrons. Previous studies suggested that enhanced convection electric fields could contribute to the earthward transport of low energy (<200 keV) electrons. However, the mechanism which leads to different efficiencies of electron transport at different energies has not been quantified. This study expands the traditional radial diffusion model with an empirically determined convection term and shows that the net convection velocity increases for lower energy electrons. For the first time, we quantitatively modeled the energy-dependent penetration of radiation belt electrons in a wide energy range (10 s of keV to 2 MeV) in the presence of enhanced large-scale electric fields, during two geomagnetic storm events observed by the Van Allen Probes mission.

1. Introduction

Energetic electrons in the inner magnetosphere are normally trapped in two regions: the inner and outer radiation belts. The inner belt is relatively stable, while the outer belt is highly dynamic, with electron fluxes varying by orders of magnitude within days during geomagnetic storms. The slot region, usually devoid of energetic electrons, separates the two belts. During geomagnetically active times, outer belt electrons can extend to lower *L* (distance to the center of Earth in units of Earth radii in the equatorial plane) and even fill the slot region (Blake et al., 1992; Li et al., 1993). The dynamic variations of radiation belt particles are the result of a complex competition between acceleration, transport, and loss mechanisms. The most important source process for inner belt electrons is inward radial transport from the outer belt (Cunningham et al., 2018; Selesnick, 2016) with cosmic ray albedo neutron decay (CRAND) contributing at the inner edge of the inner belt (Li et al., 2017; Xiang et al., 2019; Zhang et al., 2019). The energy-dependence of outer belt electrons penetrating inward can help quantify the populations of electrons transported to the inner belt during a certain event, which is important for determining source and loss processes of inner electrons. This study will focus on the mechanism responsible for the energy-dependent penetration of outer belt electrons into the low *L* region ($L < 3.5$). Our study provides

Writing – review & editing: Xinlin Li, Hong Zhao, Theodore Sarris, Lengying Khoo, Benjamin Hogan, Declan O'Brien, Sam Califf

insights into electron radiation belts from the perspective of the energy spectrum and reveals the physical mechanisms underlying radiation belt dynamics.

In-situ observations have demonstrated the storm-time penetration of outer belt electrons. Baker et al. (2004) found that compression of the outer belt's inner edge is closely associated with the reduction of the plasmasphere, the cold, dense plasma region corotating with Earth. Li et al. (2006) reported the correlation between electron enhancements and the outer plasmasphere boundary using >1 MeV electron flux measurements from SAMPEX and CRRES. Many have studied the energy-dependence of outer belt electron penetration and flux enhancements, with finer energy and temporal resolution measurements provided by the Van Allen Probes mission (Mauk et al., 2013). Reeves et al. (2016) showed that lower energy electrons penetrate the inner zone more often than higher energy electrons. Khoo et al. (2018, 2021) studied the relationship between the location of initial electron enhancement and the innermost plasmapause location during intense storms. Their results showed that initial enhancements occurred outside the innermost plasmapause, suggesting that enhanced convection is responsible for plasmasphere erosion and could contribute to lower energy electron enhancements. Mei et al. (2021) studied an energy-dependent linear relation between the upper boundary of the innermost slot region's L shell and the 15-hr-averaged K_p index. Simulations have shown that enhanced convective electric fields are likely responsible for inward transporting <200 keV electrons to lower L (Korth et al., 1999; S. Liu et al., 2003; Thorne et al., 2007; Zhao et al., 2017). Califf et al. (2017) conducted test particle simulations and showed that a large-scale electric field (E-field) with amplitudes of 1–2 mV/m can convectively transport hundreds of keV electrons and explain the observed enhancements in the slot region. It still remains an open question how to quantitatively explain and model the energy-dependent deep penetration of electrons.

In this paper, we investigate the mechanism responsible for driving lower-energy outer belt electron penetration to lower L during geomagnetic storms. We quantify the net effect of the $E \times B$ drift induced by time-variant large-scale azimuthal E-fields and consider this transport mechanism as a convection term in the radial diffusion equation for electrons at selected first adiabatic invariant, μ, values. By modifying the Volland-Stern E-field model for high K_p levels ($K_p \geq 4$), we enhance the convection E-field near Earth during storm times to match observations. Applying the modified Volland-Stern model to the convection term in 1-D diffusion-convection modeling of phase space density (PSD), we show the evolution of 10–400 MeV/G equatorial electrons during storm-time flux enhancement events. Our model achieves prediction efficiencies (PE) for lower μ electrons in the low L region ($L \sim 3$) of >∼0.9 for selected events. These results suggest the time-varying, large-scale azimuthal E-fields contributes to deeper penetration of low-energy electrons.

2. Methods

2.1. Quantification of the Energy-Dependent, E-Field-Induced Radial Transport

It is generally recognized that the azimuthal component of the convection E-field can cause electrons to move radially, but radial transport due to static E-fields will eventually negate this motion as an electron drifts around Earth. However, while the large-scale E-field enhances during storm-time, electrons with drift periods comparable to the timescales of the E-field enhancement τ_E can be transported more efficiently in the radial direction. In general, the timescale refers to the magnitude of characteristic time variations of a field quantity Q, and can be defined as $\tau = \frac{Q}{dQ/dt}$ (Roederer & Zhang, 2014); thus for E-field variations the timescale τ_E can be defined as:

$$\tau_E = \frac{E(R, \phi, t)}{|\partial E(R, \phi, t)/\partial t|} \quad (1)$$

Based on the K_p-dependent Volland-Stern E-field model, the lowest values for τ_E are found for the highest rate of change in K_p. For example, for a moderate storm in which K_p changes from 3 to 6 within 3 hr, τ_E is typically ∼1 hr at $L = 3.5$. As a comparison, the drift period for a 250 keV electron at $L = 3.5$ is ∼1 hr. Figure 1 is a schematic diagram conceptually showing how large-scale E-fields can lead to the energy-dependent radial displacement of electrons depending on the relationship between the electron drift period (τ_D) and τ_E. When $\tau_D \ll \tau_E$, the E-field can be considered nearly static during an electron's drift cycle. Shown by the red dashed drift trajectory in Figure 1, radial displacement cannot accumulate over drift cycles and the net radial transport is negligible. However, as the green dashed arc shows, when τ_D becomes comparable to τ_E, the time-varying E-field leads to imbalanced inward or outward radial drift, and thus causes considerably larger net radial motion

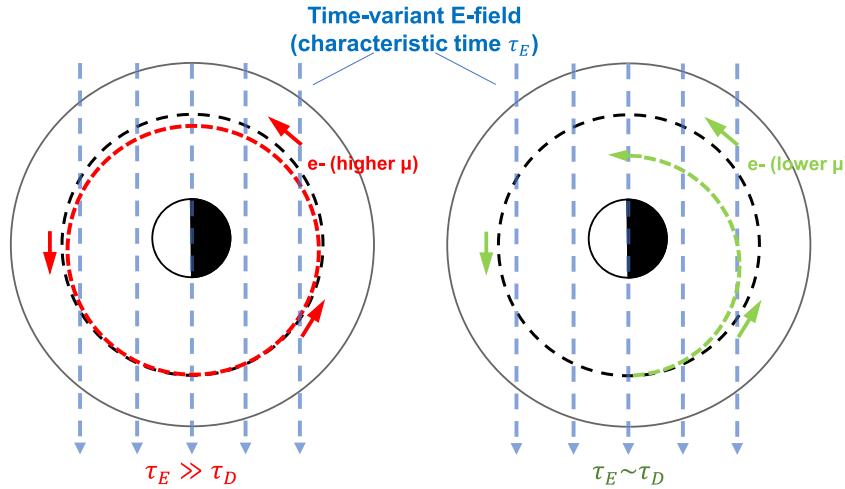

Figure 1. Demonstration of a time-varying large-scale dawn-dusk E-field leading to the energy-dependent radial transport of electrons. (Left) The E-field induced radial transport is negligible when $\tau_E \gg \tau_D$. (Right) The E-field induced radial transport becomes more efficient when $\tau_E \sim \tau_D$. Dashed blue lines represent the large-scale E-field, and the dashed black circle around Earth is the drift orbit of trapped particles. The dashed red and green curves show the drift trajectory of high μ and low μ electrons in the presence of a time-varying, large-scale E-field, respectively.

of the particle. In addition, as the first adiabatic invariant μ is conserved while the electron drifts, low μ electrons could also be transported to lower L than high μ electrons when they gain the same amount of kinetic energy due to large-scale E-field. Thus, higher energy electrons are less influenced by the time-varying E-field, and this radial transport mechanism is more important for lower energy electrons. Though azimuthal E-fields can cause electrons to radially drift inward or outward based on the azimuthal phase of an electron, the overall net effect on electron PSD is inward penetration if there is a positive radial gradient of radiation belt electron PSD. Since electron PSD at higher L for a fixed μ is normally much greater than that at lower L, only a fraction of electrons moving inward will create a significant increase in flux (Califf et al., 2017). Together with the positive radial gradient of the PSD, another important factor affecting the inward penetration of electrons is the timescale of the convective E-field variation in relation to the drift periods of electrons. Its importance can be seen in the simulation results of Califf et al. (2017), and in particular their Figure 11, where E-field pulses of different duration can be seen to affect different μ-values of electrons with an MLT dependence. With respect to the dependence of the changes in PSD on local time, it is noted that Califf et al. (2017) used symmetric distributions of particles in MLT. The $E \times B$ drift motion of electrons caused by large-scale E-fields can be described by convection processes (Aseev et al., 2016; Shprits et al., 2015). In this study, we confine the modeling to the radial dimension by providing an approximation of the net convection effect to simulate the contribution of this mechanism to electron penetration.

2.2. 1-D Modeling of Radial Diffusion and Convection

To study the radial transport induced by storm-time, time-varying E-fields and investigate their contribution to the energy-dependent penetration, we expand the traditional form of the radial diffusion Fokker-Planck equation (Schulz & Lanzerotti, 1974) by adding a convection term $V_{E\times B,\text{net}}(R,t)\frac{\partial f}{\partial L^*}$ associated with large-scale E-fields:

$$\frac{\partial f}{\partial t} = L^{*2}\frac{\partial}{\partial L^*}\left[\frac{D_{L^*L^*}}{L^{*2}}\frac{\partial f}{\partial L^*}\right] + V_{E\times B,\text{net}}(R,t)\frac{\partial f}{\partial L^*} + S - \frac{f}{\tau} \quad (2)$$

where f is the electron PSD, L^* is the Roederer L and can be calculated as: $L^* = \frac{2\pi M}{|\Phi| R_E}$ (Roederer, 1970), Φ is the third adiabatic invariant, M is the Earth's dipole magnetic moment, R is the radial distance in Earth radii, $D_{L^*L^*}$ is the radial diffusion coefficient, S is the source rate due to local heating, and τ is the electron lifetime. The convection coefficient $V_{E\times B,\text{net}}$ is an energy-dependent variable indicating the approximated net velocity of convective radial transport due to time-varying large-scale azimuthal E-fields, by assuming: (a) dipole B-field, (b)

E-field linearly changing within an 1-hr interval, (c) considering inward moving electrons in the presence of steep PSD radial gradient. An expression for $V_{E\times B,\mathrm{net}}$ is given by (derivation in Text S1 in Supporting Information S1):

$$
\begin{aligned}
V_{E\times B,\mathrm{net}} &= \left|\frac{\boldsymbol{E}_{\mathrm{net}}\times\boldsymbol{B}}{\boldsymbol{B}^2}\right| \\
\boldsymbol{E}_{\mathrm{net}} = \langle \boldsymbol{E}_\phi(R,\phi,t)\rangle_\phi \cdot \frac{\frac{1}{4}\tau_D}{\tau_E} &= \frac{\int_{\frac{\pi}{2}}^{\frac{3\pi}{2}} \boldsymbol{E}_\phi(R,\phi,t)d\phi}{\pi}\cdot\frac{\tau_D}{4\tau_E} \\
\tau_E(R,t) &= \frac{\int_{\frac{\pi}{2}}^{\frac{3\pi}{2}} E_\phi(R,\phi,t)d\phi}{\left|\frac{\partial\int_{\frac{\pi}{2}}^{\frac{3\pi}{2}} E_\phi(R,\phi,t)d\phi}{\partial t}\right|}
\end{aligned}
\tag{3}
$$

In Equation 3, $\boldsymbol{E}_{\mathrm{net}}$ approximates the time-varying large-scale E-field which can result the equivalent drift velocity $V_{E\times B,\mathrm{net}}$. $\boldsymbol{E}_\phi$ is the azimuthal component of large-scale E-field, $\boldsymbol{B}$ is the background local geomagnetic field. In this study, $\boldsymbol{E}_\phi$ and $\boldsymbol{B}$ are obtained from the Volland-Stern model and the static dipole magnetic field, respectively. ϕ is the azimuthal angle from noon. τ_E is the characteristic timescale of $\boldsymbol{E}_\phi$ averaged from dusk to dawn at a fixed L; τ_D is the electron drift period, which is a function of L and energy. Due to the energy-dependence of τ_D, the coefficient $V_{E\times B,\mathrm{net}}$ is also energy-dependent. For lower energy electrons, whose τ_D is comparable to τ_E, the convection term is more significant. As electron energy increases, τ_D decreases, and coefficient $V_{E\times B,\mathrm{net}}$ gradually diminishes, which is consistent with the concept demonstrated in Figure 1.

W. Liu et al. (2016), based on THEMIS observations, developed an expression for a μ-dependent radial diffusion coefficient, $D^E_{LL,\mathrm{Liu}}$, for electrons with $\mu = 400$–$8{,}000$ MeV/G, higher than the μ-range (<400 MeV/G) considered herein. The expression used in W. Liu et al. (2016) is:

$$
D^E_{LL,\mathrm{Liu}} = 1.115\cdot 10^{-6}\cdot 10^{0.281\times Kp}\cdot L^{8.184}\cdot \mu^{-0.608} \tag{4}
$$

To apply the $D^E_{LL,\mathrm{Liu}}$ for 100 s keV electron energy-dependent modeling, the expression by W. Liu et al. (2016) is extended to lower μ ranges (10–400 MeV/G) and modified as a function of K_p and μ. The modified $D_{LL,\mathrm{Liu}}$ model we used is:

$$
\begin{aligned}
D^E_{LL,\mathrm{Liu-mod}} &= 1.115\cdot 10^{-6}\cdot 10^{a\times K_\mathrm{p}+b}\cdot L^{8.184}\cdot \mu^c\cdot d \\
a &= 0.35; b = -0.414; \\
c &= -0.57; d = 0.796
\end{aligned}
\tag{5}
$$

where μ is the first adiabatic invariant of the electron in MeV/G, a, b, c, d are parameters to modify the expression of $D^E_{LL,\mathrm{Liu-mod}}$. More specifically, a and c are two free parameters adjusting the $D_{LL,\mathrm{Liu}}$ model as a function of K_p and μ, parameters b and d are dependently determined by maintaining the continuity of $D_{LL,\mathrm{Liu}}$ at 400 MeV/G and $K_\mathrm{p} = 6$. The optimal values for the parameters are determined by searching for the best overall performance of the "radial diffusion-only"-modeled electron PSD compared to observed PSD over a wide range of $\mu < 400$ MeV/G (see Text S3 in Supporting Information S1).

For modeling with Equation 2, we set the source term $S = 0$ for our model, as local heating effects are not considered in this study since we focus on the energization of lower energy electrons by inward radial transport. The time step for computing the model is 3-min. The empirical models of electron lifetime due to chorus wave or hiss wave pitch angle scattering are applied to determine the loss term $-\frac{f}{\tau}$ (Gu et al., 2012; Zhu et al., 2021). Inside the empirical plasmapause location (Carpenter & Anderson, 1992), the electron lifetime is dominated by τ_{hiss} obtained from the empirical model of slot region hiss induced electron loss timescales by Zhu et al. (2021), while outside the plasmapause, we use the electron lifetime τ_{chorus} parameterized by Gu et al. (2012). The 4.5-hr

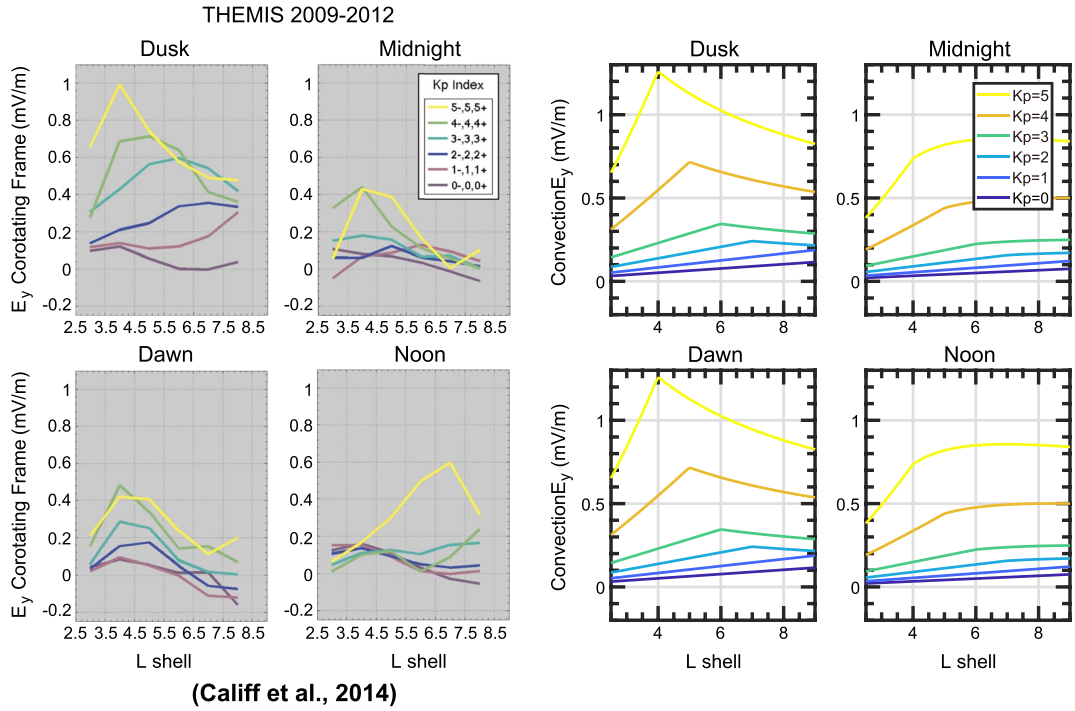

Figure 2. (Left) Radial profiles of the dawn-dusk E-field according to Califf et al. (2014) in the frame corotating with Earth, as a function of L, for select K_p values, in the dusk, midnight, dawn and noon regions, as marked. (Right) Radial profiles of the modified Volland-Stern model convection E-field as a function of L, for select K_p values, and for the same local time regions as the left-hand side panels.

resolution PSD derived from flux observation at the highest available L is used as the outer boundary condition for the 4.5-hr intervals, while a constant inner boundary condition is used at ~1.1 R_E. When the highest available L increases, PSD is interpolated to fill the gap.

2.3. Modification on the Volland-Stern E-Field Model

Enhanced convection E-fields can lead to the erosion of the plasmasphere, which could also cause electrons to penetrate to lower L. Motivated by the discrepancies between the Volland-Stern model (Maynard & Chen, 1975; Stern, 1975; Volland, 1973) and statistical observations of large-scale E-field during active times (Califf et al., 2014), we modify the Volland-Stern model at higher K_p by increasing storm-time convection E-fields near Earth. Figure 2 shows the comparison between a statistical study of the dawn-dusk component of the E-field (E_y) from Califf et al. (2014) and our modified Volland-Stern model. Statistics show that E_y during times of high K_p can reach a local maximum at low L, especially in the dusk sector. Despite the discrepancies like the dawn-dusk asymmetry, we create a similar local maximum E_y to mimic the statistical results on the nightside at low L. The modification on the Volland-Stern model follows the piecewise functions:

$$\Phi = \begin{cases} -\dfrac{92.4}{R} - AR^N \sin\phi\,(kV), & \left(R < R_t\left(K_p\right)\right) \\ -\dfrac{92.4}{R} - A\left(a_E R^{\frac{0.8}{N}} + b_E\right)\sin\phi\,(kV), & \left(R \geq R_t\left(K_p\right)\right) \end{cases} \tag{6}$$

$$N = \begin{cases} 2.2, \left(4 < K_p \leq 5\right) \\ 2.4, \left(5 < K_p \leq 6\right) \end{cases}$$

In Equation 6, Φ is the electric potential, R is the radial distance, ϕ is the azimuthal angle from noon, A is given by Maynard and Chen (1975): $A = \frac{0.045}{\left(1-0.159K_p+0.0093{K_p}^2\right)^3}\left(\frac{kV}{R_E^2}\right)$, R_t is the radial distance in Earth radii where the

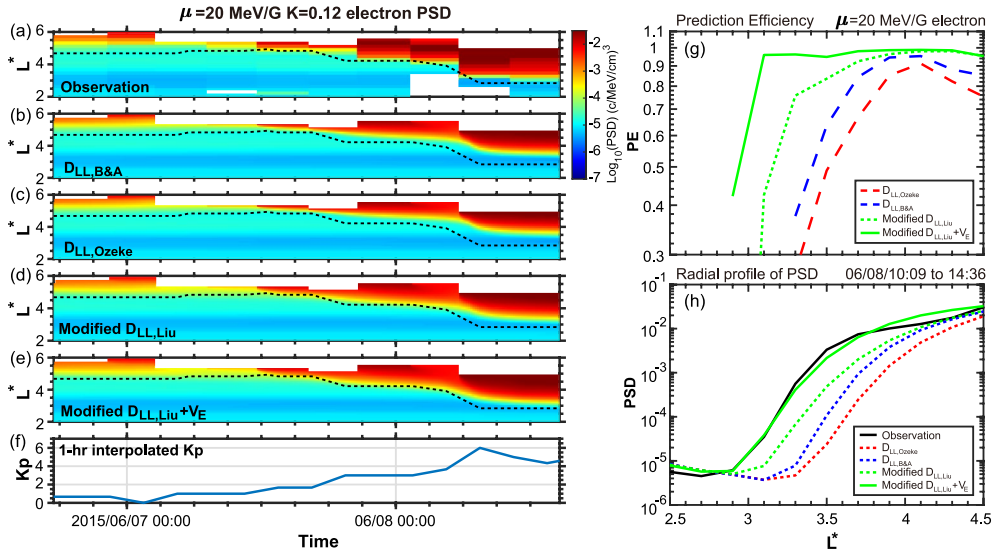

Figure 3. Comparisons between observed and modeled phase space density (PSD) for $\mu = 20\,\mathrm{MeV/G}$, $K = 0.12G^{1/2}R_E$ electrons from 7 to 9 June 2015. (a) PSD calculated from RBSP A&B flux observations; (b) Modeled PSD with $D_{LL,B\&A}$; (c) with $D_{LL,\mathrm{Ozeke}}$; (d) with $D_{LL,\mathrm{Liu-mod}}$; (e) with $D_{LL,\mathrm{Liu-mod}}$ and V_E; (f) K_p index; (g) prediction efficiency as a function of L^* with different coefficients; (h) PSD radial profile comparisons during the initial enhancement.

local maximum dawn-dusk E-field component E_y is observed as a function of K_p according to Califf et al. (2014). Coefficients a_E and b_E are applied to make $\Phi(R)$ and $\frac{\partial\Phi(R)}{\partial R}$ continuous, thus $E(R)$ will also be continuous (see Table S1 in Supporting Information S1 for values of R_t, a_E, and b_E). Parameter N is set equal to 2 in Volland-Stern model, but it is modified as a function of K_p in this study to produce an enhanced E-field near Earth during active times. When $K_\mathrm{p} \le 4$, we use the original Volland-Stern model. At more disturbed times when $K_\mathrm{p} > 4$, the modified Volland-Stern model is used to enhance the convection E-field with larger N values according to Equation 6. The above model is a time-varying convection electric field, that is parameterized according to 1-hr interpolated K_p.

3. Results

A moderate storm on 8 June 2015 is studied to investigate whether convective radial transport resulted by large-scale E-field can explain the deep penetration of lower energy electrons. During the event, the minimum Dst index is −73 nT and the maximum K_p is 6.

Figure 3 shows the comparison between the observed PSD for 20 MeV/G, $K = 0.12\,G^{1/2}R_E$ electrons computed from RBSP A& B flux measurements (Blake et al., 2013) using the T89D model (Tsyganenko, 1989) (panel a), modeled PSD with different coefficient sets (panels b through e), the prediction efficiency (PE) for the various models with different coefficient sets for the presented period (panel f), and radial profiles of PSD during the initial enhancement (panel g). Comparisons at other μ values are shown in the Supporting Information. Three groups of radial-diffusion-only modeling are conducted with the μ-independent coefficients $D_{LL,B\&A}$ (Brautigam & Albert, 2000), $D_{LL,\mathrm{Ozeke}}$ (Ozeke et al., 2014), and the μ-dependent coefficient $D_{LL,\mathrm{Liu-mod}}$ given by Equation 5. The test group is a diffusion-convection model with the same $D_{LL,\mathrm{Liu-mod}}$ and with the additional convection term where V_E is given by Equation 3, aiming to illustrate the relative contribution of the energy-dependent convection term V_E. Prediction efficiency is defined as:

$$\mathrm{PE} = 1 - \frac{\text{mean square residual}}{\text{variance of data}} = 1 - \frac{\sum_i^n (m_i - p_i)^2}{\sum_i^n \left(m_i - \overline{m}\right)^2} \tag{7}$$

where m_i and p_i respectively denote the observed and modeled log (PSD), $\overline{m}$ is the mean of m_i. In this study, PE is calculated for a 1-day period during the PSD enhancement. Positive PE values suggest better prediction than the average value (e.g., Barker et al., 2005; Li et al., 2001). Black dotted lines in Figure 3a–3e show the innermost

plasmapause location determined by the Carpenter and Anderson (1992) empirical model. In Figure 3a, the observations show PSD enhancements by at least 2 orders of magnitude outside the plasmapause (which is $L \sim 3$ during the event). Figure 3g-3h show that "radial diffusion-only"-modeling based on any of the $D_{LL,B\&A}$, $D_{LL,\mathrm{Ozke}}$ or $D_{LL,\mathrm{Liu-mod}}$ diffusion coefficients is not sufficient to create the observed PSD enhancement near the plasmapause, whereas the modeling results with both diffusive and convective radial transport using the combination of $D_{LL,\mathrm{Liu-mod}}$ and V_E provide an enhancement that is comparable to the observations. Furthermore, PE values of pure radial diffusion modeling with $D_{LL,\mathrm{Liu-mod}}$ drop to below 0.9 for $L < 3.5$ and eventually drop to negative values when approaching the plasmapause at $L \sim 3$, while radial PSD values are constantly lower than the observed PSD by one order of magnitude in the region $L \cong 3$–3.5. These suggest that radial diffusion alone cannot provide sufficient electron penetration to lower L ($L \cong 3$–3.5) for low μ electrons. When the convective radial transport is considered, PE performance is significantly improved especially for $L \sim 3$ near the innermost edge of the observed enhancement. The results suggest that the large-scale E-fields play an important role to radially transporting low μ electrons to lower L.

To illustrate the energy-dependent electron penetration, we convert the modeled 10–400 MeV/G, $K = 0.12\,G^{1/2}R_E$ electron PSD to differential flux with the T89D model and compare the modeled flux with electron flux measurements. In Figure 4, electron fluxes are displayed as a function of L and energy. The left column shows the observed 70° local pitch angle electron flux profiles during each half orbit pass, the middle column shows the modeled electron flux with μ-independent $D_{LL,\mathrm{Ozeke}}$ at epochs between the corresponding timespan of observations, and the right column shows the modeled electron flux with μ-dependent $D_{LL,\mathrm{Liu-mod}}$ and V_E terms. During this period the outer belt electron fluxes were significantly enhanced and electrons were transported to $L \sim 3$–4. Electrons with energy <200 keV move inward to the slot region and the radiation belts develop a "V" shaped structure as these lower energy outer belt electrons penetrate to lower L. The diffusion-only model with $D_{LL,\mathrm{Ozeke}}$ in the middle panel cannot reproduce the "V" shaped structure, and lower energy electrons cannot reach $L \sim 3$–3.5 when only driven by radial diffusion, similar results are obtained with the $D_{LL,B\&A}$ and $D_{LL,\mathrm{Liu-mod}}$ (not shown herein). Diffusion-convection modeling with the V_E term, shown in the right panel, reproduces the energy-dependent electron penetration better and captures the slot region filling features for <200 keV electrons, including the "V" shaped structure. It is noted that Ripoll et al. (2016) reproduced the formation of "S" shaped structure during quiet time due to the post-storm energy-dependent electron decay. Our study suggests that enhanced convection plays an important role on the formation of "V" shaped structures, as those of Figure 4, and in the storm-time energy-dependent inward penetration and energization of low energy electrons.

To further examine the diffusion-convection model and the mechanism responsible for energy-dependent penetration, another moderate storm on 4 November 2014 is studied. During this event, the minimum Dst is −44 nT and maximum K_p is 4+. Parameters for $D_{LL,\mathrm{Liu-mod}}$ and the modified Volland-Stern model are kept the same as those in the 8 June 2015 event. As the Figure S6 in Supporting Information S1 shows, PE for modeled lower μ electron PSD is significantly improved to greater than 0.6 near the inner edge of the outer belt with combination of the V_E and $D_{LL,\mathrm{Liu-mod}}$. Radial profiles of 10–60 MeV/G electron PSD with the convective term V_E better reproduces that of observations while diffusion-only modeling with μ-independent D_{LL} is not sufficient to move electrons inward to $L < \sim 3$. The good comparison with the electron flux variations in Figure S7 in Supporting Information S1 further shows the contribution of enhanced convection on low energy electron penetrations.

4. Discussion and Conclusion

This study investigates the mechanism of energy-dependent outer belt electron penetration by conducting simulations over a broad energy range and extending the general radial diffusion model with an additional convection term determined by a time-variant large-scale E-field model. The results suggest that the convective transport effect due to time-variant large-scale E-fields is responsible for the deep inward penetration of lower (<500 keV) energy electrons. Higher energy electrons with shorter drift periods are less affected. In this study, the scenario where the large-scale E-field varies on shorter timescales than that of the electron drift period ($\tau_E \ll \tau_D$), such as shock-induced E-field impulses, is not addressed.

Both events studied correspond to moderate storms with maximum $K_p \leq 6$. Previous studies (Liemohn & Jazowski, 2008; Menz et al., 2019) suggested that the performance of the Volland-Stern E-field model is better when $K_p < 7$. The modified Volland-Stern model mimics the trend of large-scale E-fields at low L from statistics by Califf et al. (2014), which also concentrated on $K_p < 6$. Based on the assumptions made,

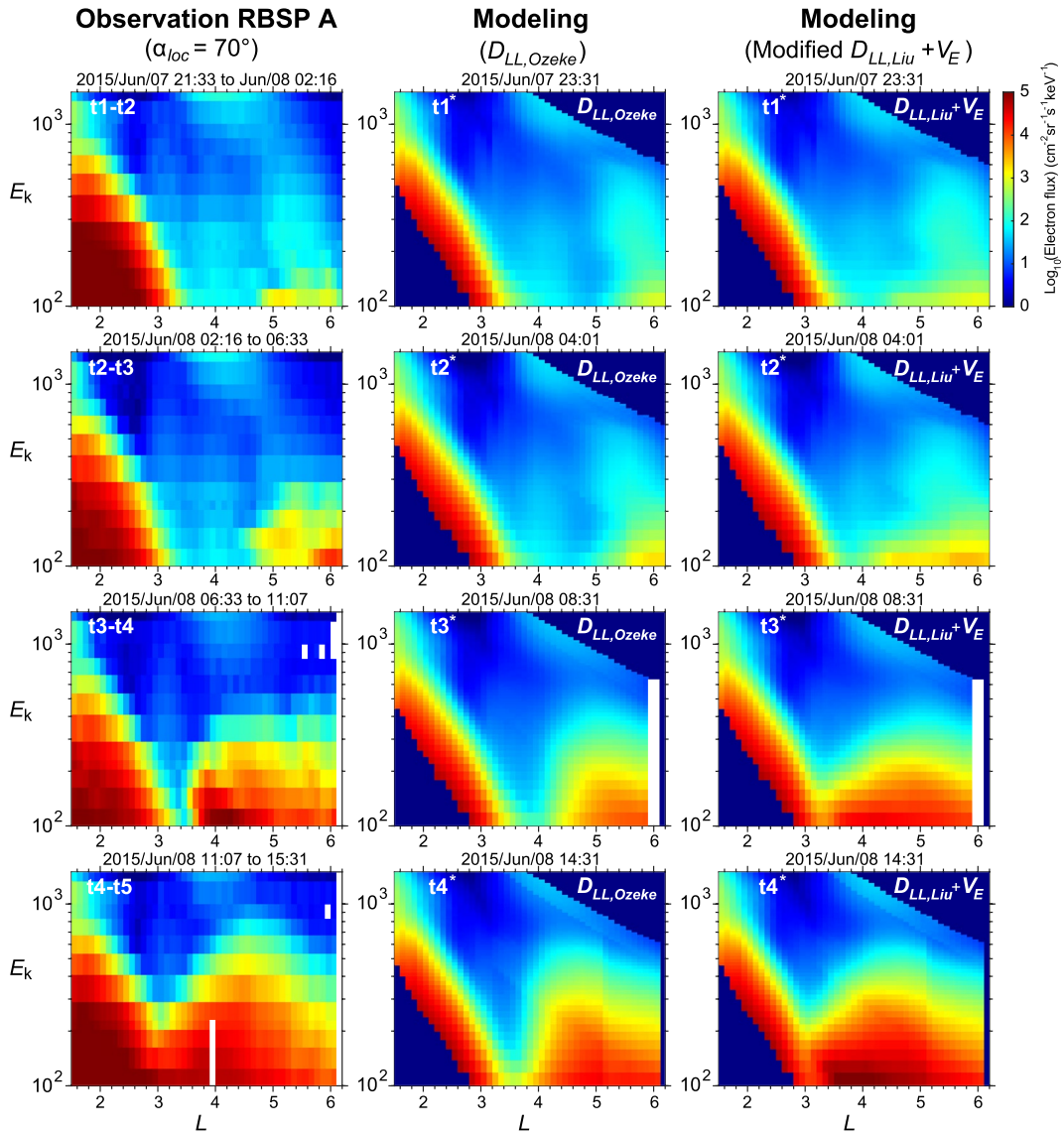

Figure 4. Electron flux variations as a function of kinetic energy and L shell. (left column) Pass-averaged fluxes of $\alpha_{\rm loc} = 70°$ electrons observed by RBSP A on 8 June 2015; (middle column) Modeled electron fluxes for $K = 0.12G^{1/2}R_E$ with $D_{LL,\rm Ozeke}$; (right column) Modeled electron fluxes with $D_{LL,\rm Liu-mod}$ and V_E.

the diffusion-convection model confined to the radial dimension for simplicity is suitable for studying radial transporting electrons at low L during moderate storms. As Figure S9 in Supporting Information S1 shows, locally observed PSD suggest an MLT-dependent electron deep penetration at short timescales. A drift-resolved Fokker-Planck code, which would allow investigating the MLT-dependent PSD time-evolution, is beyond the scope of this study.

The results of this study can be summarized as follows:

1. The energy-dependence of outer radiation belt electron penetration depth can be explained by the relationship between the large-scale azimuthal E-field variation timescale and the drift period of electrons at different energies and radial locations. Higher energy electrons with much shorter drift periods are less affected by the convection E-field, while 10–100 s of keV electrons are moved deeper inward as a result of the combination of the convective and diffusive effects.
2. Time-varying large-scale azimuthal E-fields must be considered to model the deep penetration of lower μ electrons. By introducing a convection term determined by a modified Volland-Stern E-model on top of the

radial diffusion modeling, prediction efficiencies of the modeled PSD for 10–100 MeV/G electrons at low L-shells are significantly improved compared to when using only radial diffusion modeling.

Data Availability Statement

We acknowledge the Van Allen Probes mission, particularly the ECT team for providing the particle data. Processing and analysis of the MagEIS data was supported by Energetic Particle, Composition, and Thermal Plasma (RBSP-ECT) investigation funded under NASA's Prime contract no. NAS5-01072. All RBSP-ECT data are publicly available at https://rbsp-ect.newmexicoconsortium.org/science/DataDirectories.php. The geomagnetic indices were obtained from the OMNI database (https://omniweb.gsfc.nasa.gov).

Acknowledgments
This work is supported by NSF Grant AGS 1834971 and NASA Grants 80NSSC19K0995 and 80NSSC21K0583. H. Zhao was supported by the NSF Grant AGS 2140934 and NASA Grant 80NSSC22K0356.

References

Aseev, N. A., Shprits, Y. Y., Drozdov, A. Y., & Kellerman, A. C. (2016). Numerical applications of the advective-diffusive codes for the inner magnetosphere. *Space Weather*, *14*(11), 993–1010. https://doi.org/10.1002/2016SW001484

Baker, D. N., Kanekal, S. G., Li, X., Monk, S. P., Goldstein, J., & Burch, J. L. (2004). An extreme distortion of the Van Allen belt arising from the 'Hallowe'en' solar storm in 2003. *Nature*, *432*(7019), 878–881. https://doi.org/10.1038/nature03116

Barker, A. B., Li, X., & Selesnick, R. S. (2005). Modeling the radiation belt electrons with radial diffusion driven by the solar wind. *Space Weather*, *3*(10), S10003. https://doi.org/10.1029/2004SW000118

Blake, J. B., Carranza, P. A., Claudepierre, S. G., Clemmons, J. H., Crain, W. R., Dotan, Y., et al. (2013). The magnetic electron ion spectrometer (MagEIS) instruments aboard the Radiation Belt Storm Probes (RBSP) spacecraft. *Space Science Reviews*, *179*(1–4), 383–421. https://doi.org/10.1007/s11214-013-9991-8

Blake, J. B., Kolasinski, W. A., Fillius, R. W., & Mullen, E. G. (1992). Injection of electrons and protons with energies of tens of MeV into $L < 3$ on 24 March 1991. *Geophysical Research Letters*, *19*(8), 821–824. https://doi.org/10.1029/92gl00624

Brautigam, D. H., & Albert, J. M. (2000). Radial diffusion analysis of outer radiation belt electrons during the October 9, 1990, magnetic storm. *Journal of Geophysical Research*, *105*(A1), 291–309. https://doi.org/10.1029/1999ja900344

Califf, S., Li, X., Blum, L., Jaynes, A., Schiller, Q., Zhao, H., et al. (2014). THEMIS measurements of quasi-static electric fields in the inner magnetosphere. *Journal of Geophysical Research: Space Physics*, *119*(12), 9939–9951. https://doi.org/10.1002/2014ja020360

Califf, S., Li, X., Zhao, H., Kellerman, A., Sarris, T. E., Jaynes, A., & Malaspina, D. M. (2017). The role of the convection electric field in filling the slot region between the inner and outer radiation belts. *Journal of Geophysical Research: Space Physics*, *122*(2), 2051–2068. https://doi.org/10.1002/2016ja023657

Carpenter, D. L., & Anderson, R. R. (1992). An ISEE/whistler model of equatorial electron density in the magnetosphere. *Journal of Geophysical Research*, *97*(A2), 1097–1108. https://doi.org/10.1029/91JA01548

Cunningham, G. S., Loridan, V., Ripoll, J.-F., & Schulz, M. (2018). Neoclassical diffusion of radiation-belt electrons across very LowL-shells. *Journal of Geophysical Research: Space Physics*, *123*(4), 2884–2901. https://doi.org/10.1002/2017ja024931

Gu, X., Shprits, Y. Y., & Ni, B. (2012). Parameterized lifetime of radiation belt electrons interacting with lower-band and upper-band oblique chorus waves. *Geophysical Research Letters*, *39*(15), 15102. https://doi.org/10.1029/2012gl052519

Khoo, L. Y., Li, X., Zhao, H., Sarris, T. E., Xiang, Z., Zhang, K., et al. (2018). On the initial enhancement of energetic electrons and the innermost plasmapause locations: Coronal Mass ejection-driven storm periods. *Journal of Geophysical Research: Space Physics*, *123*(11), 9252–9264. https://doi.org/10.1029/2018ja026074

Khoo, L. Y., Li, X., Zhao, H., Thaller, S. A., & Hogan, B. (2021). Multi-event studies of sudden energetic electron enhancements in the inner magnetosphere and its association with plasmapause positions. *Journal of Geophysical Research: Space Physics*, *126*(11), e2021JA029769. https://doi.org/10.1029/2021ja029769

Korth, H., Thomsen, M. F., Borovsky, J. E., & McComas, D. J. (1999). Plasma sheet access to geosynchronous orbit. *Journal of Geophysical Research*, *104*(A11), 25047–25061. https://doi.org/10.1029/1999ja900292

Li, X., Baker, D. N., O'Brien, T. P., Xie, L., & Zong, Q. G. (2006). Correlation between the inner edge of outer radiation belt electrons and the innermost plasmapause location. *Geophysical Research Letters*, *33*(14), L14107. https://doi.org/10.1029/2006gl026294

Li, X., Roth, I., Temerin, M., Wygant, J. R., Hudson, M. K., & Blake, J. B. (1993). Simulation of the prompt energization and transport of radiation belt particles during the March 24, 1991 SSC. *Geophysical Research Letters*, *20*(22), 2423–2426. https://doi.org/10.1029/93GL02701

Li, X., Selesnick, R., Schiller, Q., Zhang, K., Zhao, H., Baker, D. N., & Temerin, M. A. (2017). Measurement of electrons from albedo neutron decay and neutron density in near-earth space. *Nature*, *552*(7685), 382–385. https://doi.org/10.1038/nature24642

Li, X., Temerin, M., Baker, D. N., Reeves, G. D., & Larson, D. (2001). Quantitative prediction of radiation belt electrons at geostationary orbit based on solar wind measurements. *Geophysical Research Letters*, *28*(9), 1887–1890. https://doi.org/10.1029/2000GL012681

Liemohn, M. W., & Jazowski, M. (2008). Ring current simulations of the 90 intense storms during solar cycle 23. *Journal of Geophysical Research*, *113*(A3), A00A17. https://doi.org/10.1029/2008ja013466

Liu, S., Chen, M. W., Lyons, L. R., Korth, H., Albert, J. M., Roeder, J. L., et al. (2003). Contribution of convective transport to stormtime ring current electron injection. *Journal of Geophysical Research*, *108*(A10), 1372. https://doi.org/10.1029/2003ja010004

Liu, W., Tu, W., Li, X., Sarris, T., Khotyaintsev, Y., Fu, H., et al. (2016). On the calculation of electric diffusion coefficient of radiation belt electrons with in situ electric field measurements by THEMIS. *Geophysical Research Letters*, *43*(3), 1023–1030. https://doi.org/10.1002/2015gl067398

Mauk, B. H., Fox, N. J., Kanekal, S. G., Kessel, R. L., Sibeck, D. G., & Ukhorskiy, A. (2013). Science objectives and rationale for the radiation belt storm probes mission. *Space Science Reviews*, *179*(1–4), 3–27. https://doi.org/10.1007/s11214-012-9908-y

Maynard, N. C., & Chen, A. J. (1975). Isolated cold plasma regions: Observations and their relation to possible production mechanisms. *Journal of Geophysical Research*, *80*(7), 1009–1013. https://doi.org/10.1029/ja080i007p01009

Mei, Y., Ge, Y., Du, A., Gu, X., Summers, D., Li, X., et al. (2021). Energy-dependent boundaries of earth's radiation belt electron slot region. *The Astrophysical Journal*, *922*(2), 246. https://doi.org/10.3847/1538-4357/ac25ec

Menz, A. M., Kistler, L. M., Mouikis, C. G., Spence, H. E., & Henderson, M. G. (2019). Effects of a realistic O+ source on modeling the ring current. *Journal of Geophysical Research: Space Physics*, *124*(12), 9953–9962. https://doi.org/10.1029/2019ja026859

Ozeke, L. G., Mann, I. R., Murphy, K. R., Jonathan Rae, I., & Milling, D. K. (2014). Analytic expressions for ULF wave radiation belt radial diffusion coefficients. *Journal of Geophysical Research: Space Physics*, *119*(3), 1587–1605. https://doi.org/10.1002/2013ja019204

Reeves, G. D., Friedel, R. H., Larsen, B. A., Skoug, R. M., Funsten, H. O., Claudepierre, S. G., et al. (2016). Energy-dependent dynamics of keV to MeV electrons in the inner zone, outer zone, and slot regions. *Journal of Geophysical Research: Space Physics*, *121*(1), 397–412. https://doi.org/10.1002/2015ja021569

Ripoll, J.-F., Reeves, G. D., Cunningham, G. S., Loridan, V., Denton, M., Santolik, O., et al. (2016). Reproducing the observed energy-dependent structure of earth's electron radiation belts during storm recovery with an event-specific diffusion model. *Geophysical Research Letters*, *43*(11), 5616–5625. https://doi.org/10.1002/2016gl068869

Roederer, J. G. (1970). *Dynamics of geomagnetically trapped radiation*. Springer-Verlag.

Roederer, J. G., & Zhang, H. (2014). Dynamics of magnetically trapped particles. In *Foundations of the physics of radiation belts and space plasmas*.

Schulz, M., & Lanzerotti, J. (1974). Particle diffusion in the radiation belts.

Selesnick, R. S. (2016). Stochastic simulation of inner radiation belt electron decay by atmospheric scattering. *Journal of Geophysical Research: Space Physics*, *121*(2), 1249–1262. https://doi.org/10.1002/2015ja022180

Shprits, Y. Y., Kellerman, A. C., Drozdov, A. Y., Spence, H. E., Reeves, G. D., & Baker, D. N. (2015). Combined convective and diffusive simulations: VERB-4D comparison with 17 March 2013 Van allen Probes observations. *Geophysical Research Letters*, *42*(22), 9600–9608. https://doi.org/10.1002/2015gl065230

Stern, D. P. (1975). The motion of a proton in the equatorial magnetosphere. *Journal of Geophysical Research*, *80*(4), 595–599. https://doi.org/10.1029/ja080i004p00595

Thorne, R. M., Shprits, Y. Y., Meredith, N. P., Horne, R. B., Li, W., & Lyons, L. R. (2007). Refilling of the slot region between the inner and outer electron radiation belts during geomagnetic storms. *Journal of Geophysical Research*, *112*(A6), A06203. https://doi.org/10.1029/2006ja012176

Tsyganenko, N. A. (1989). A magnetospheric magnetic field model with a warped tail current sheet. *Planetary and Space Science*, *37*(1), 5–20. https://doi.org/10.1016/0032-0633(89)90066-4

Volland, H. (1973). A semiempirical model of large-scale magnetospheric electric fields. *Journal of Geophysical Research*, *78*(1), 171–180. https://doi.org/10.1029/ja078i001p00171

Xiang, Z., Li, X., Selesnick, R., Temerin, M. A., Ni, B., Zhao, H., et al. (2019). Modeling the quasi-trapped electron fluxes from cosmic ray albedo neutron decay (CRAND). *Geophysical Research Letters*, *46*(4), 1919–1928. https://doi.org/10.1029/2018gl081730

Zhang, K., Li, X., Zhao, H., Schiller, Q., Khoo, L. Y., Xiang, Z., et al. (2019). Cosmic ray albedo neutron decay (CRAND) as a source of inner belt electrons: Energy spectrum study. *Geophysical Research Letters*, *46*(2), 544–552. https://doi.org/10.1029/2018gl080887

Zhao, H., Baker, D. N., Califf, S., Li, X., Jaynes, A. N., Leonard, T., et al. (2017). Van allen Probes measurements of energetic particle deep penetration into the low L region ($L < 4$) during the storm on 8 April 2016. *Journal of Geophysical Research: Space Physics*, *122*(12), 12-140. https://doi.org/10.1002/2017ja024558

Zhu, Q., Cao, X., Gu, X., Ni, B., Xiang, Z., Fu, S., et al. (2021). Empirical loss timescales of slot region electrons due to plasmaspheric hiss based on Van Allen Probes Observations. *Journal of Geophysical Research: Space Physics*, *126*(4), e2020JA029057. https://doi.org/10.1029/2020JA029057